Functionalized Ultrasound-Propelled Magnetically Guided Nanomotors: Toward Practical Biomedical Applications

Victor Garcia-Gradilla, Jahir Orozco, Sirilak Sattayasamitsathit, Fernando Soto, Filiz Kuralay, Ashley Pourazary, Adlai Katzenberg, Wei Gao, Yufeng Shen, and Joseph Wang*

Department of Nanoengineering, University of California, San Diego, La Jolla, California 92093, United States

ABSTRACT Magnetically guided ultrasound-powered nanowire motors, functionalized with bioreceptors and a drug-loaded polymeric segment, are described for "capture and transport" and drug-delivery processes. These high-performance fuel-free motors display advanced capabilities and functionalities, including magnetic guidance, coordinated aligned movement, cargo towing, capture and isolation of biological targets, drug delivery, and operation in real-life biological and environmental media. The template-prepared three-segment Au—Ni—Au nanowire motors are propelled acoustically by mechanical waves produced by a piezoelectric transducer. An embedded nickel segment facilitates a magnetically guided motion as well as transport of large "cargo" along predetermined trajectories. Substantial improvement in the speed and power is realized by the controlled concavity formation at the end of the motor nanowire using a sphere lithography protocol. Functionalization of the Au segments with lectin and antiprotein A antibody bioreceptors allows capture and transport of *E. coli* and *S. aureus* bacteria, respectively. Potential therapeutic applications are illustrated in connection to the addition of a pH-sensitive drug-loaded polymeric (PPy-PSS) segment. The attractive capabilities of these fuel-free acoustically driven functionalized Au—Ni—Au nanowires, along with the simple preparation procedure and minimal adverse effects of ultrasonic waves, make them highly attractive for diverse *in vivo* biomedical applications.

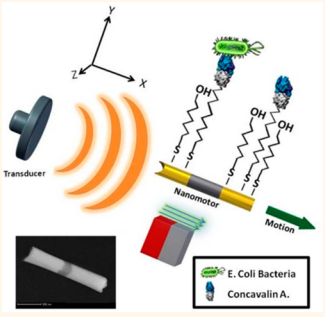

KEYWORDS: nanomotors · ultrasound · magnetic · sphere lithography · drug delivery

The use of nanomotors to power nanomachines is currently a research area of intense activity due to numerous potential applications, ranging from directed drug delivery to nanoscale fabrication.[1−9] Synthetic nanomotors, based on a multitude of propulsion mechanisms, have thus been developed. While most of this attention has been given to chemically powered catalytic motors,[3,4,8] many important applications (particularly *in vivo* biomedical ones) require the elimination of the fuel requirements toward biocompatible propulsion mechanisms. Efforts in this direction have led to the fuel-free locomotion of magnetically driven nanoswimmers,[10−12] or electrically propelled devices.[13−15] Recently introduced ultrasound (US)-driven propulsion mechanisms greatly enhance the prospects for biomedical applications of small scale machines.[16−18] For example, Wang and Esener developed efficient "microbullets" that utilize ultrasound to externally trigger ultrafast velocity and remarkable thrust for deep tissue penetration and deformation.[16] Hoyos and Mallouk described the acoustically driven movement of gold nanowires, associated with a local pressure gradient formed in the concave ends of the wires by the applied ultrasound waves.[17] Such biocompatible ultrasound locomotion schemes offer considerable promise for diverse biomedical applications, reflecting the widespread use of ultrasound in medicine.[18−20]

Here we demonstrate ultrasound-powered nanowire motors with a variety of new capabilities and functionalities and a greatly enhanced performance, for diverse practical biomedical applications. Such new capabilities of these acoustically driven nanomotors include magnetic guidance, cargo towing, locomotion in unprocessed

* Address correspondence to josephwang@ucsd.edu.

Received for review July 24, 2013 and accepted August 22, 2013.

Published online August 23, 2013
10.1021/nn403851v

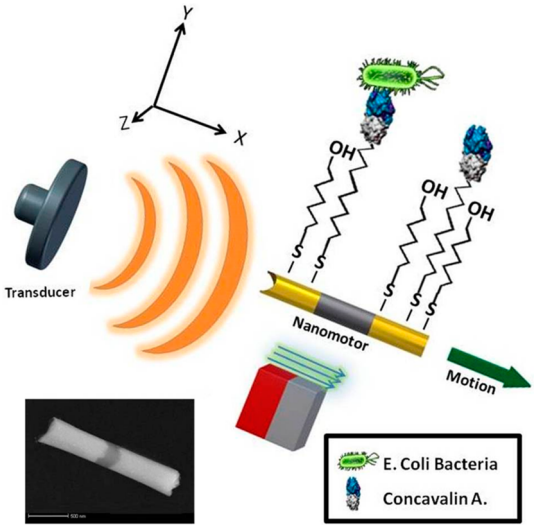

Figure 1. Ultrasound-propelled magnetically guided receptor-functionalized nanowire motor for selective capture and transport of biological targets.

real-life media, sorting of biological targets, and drug delivery. As illustrated in Figure 1, such attractive performance has been realized by functionalizing the gold surface of the motor with various bioreceptors (antibody or lectin) for "on-the-fly" capture and transport of biological targets, and incorporating an additional pH-sensitive drug-loaded polymeric segment, and a magnetized Ni segment for directional motion, coordinated group movement, and cargo loading and manipulation. Such use of ultrasound-driven (fuel-free) nanomotors can address the limitations of peroxide-powered micromotors in maintaining the viability of the captured biological target or in-body therapeutic applications. The resulting nanomachine is capable of targeting and transporting diverse cargo as well as releasing drugs in response to specific stimuli, all while moving in a controlled and cooperative fashion that is not limited by the surrounding environment or harmful to biological media. The new US-driven multisegment Au/Ni/Au/PPy nanowire motors can be mass produced using a simple template electrodeposition protocol. Such development of highly efficient and controllable multifunctional medically safe acoustically driven nanomotors offers great promise for future *in vivo* biomedical applications.

RESULTS AND DISCUSSION

The acoustically propelled nanomotors have been fabricated through a template electrodeposition method and are composed of a 0.25 μm diameter, 1.8 μm long three-segment Au/Ni/Au (0.8 μm/0.2 μm/0.8 μm) nanowire. A copper sacrificial layer was deposited first for the creation of a concave shape cavity in one end of the nanomotor. The nanowires rise to a levitation plane and propel from the pressure gradient generated by the ultrasound waves penetrating their concave end (Figure 1), in accordance with early findings of Mallouk's team.[17] The embedded Ni segment offers convenient magnetic alignment, thus allowing the nanomotors to be guided along predetermined trajectories. Modification of the nanomotor gold surface with a mixed self-assembly monolayer (SAM) of 11-mercaptoundecanoic acid (MUA) and 6-mercaptohexanol (MCH) facilitates functionalization of specific bioreceptors to selectively capture *E. coli* or *S. aureus* bacteria in complex media (Figure 1).

The incorporation of nickel segments has been previously used for magnetic alignment of chemically powered nanowire motors.[21,22] In the present work, the US-propelled wire motors have been oriented in the direction of an external magnetic field produced by a Neodymium magnet. Figure 2A and corresponding SI Video 1 illustrate the effect of the magnetic field on the directional movement of the US-driven nanowires. For example, the motor is initially moving straight by aligning with the magnetic field (a); turning the field "off" results in a random movement, with a spiral trajectory (b). Finally, restoring the magnetic field leads to a resumed straight-line aligned motion (c). Directional movement over more complex trajectories and at all angles is also possible by changing the orientation of the applied magnetic field while the nanomotor is propelled acoustically. Figure 2B and SI Video 2 illustrate the "writing" of UCSD letters by the ultrasound propelled nanomotors under magnetic guidance. The individual motors thus follow the predetermined (U, C, S, D) trajectories at a constant speed, without affecting the actual US-driven motion. The magnetic guidance also facilitates the coordinated collective movement of multiple US-based motors. For example, Figure 2C and corresponding SI Video 3 illustrate the organized coordinated movement of a group of four US-driven nanomotors. These motors move along a common trajectory at a comparable speed, as guided by the continuously changing direction of the magnetic field. Such collective motion could benefit challenging biomedical tasks, ranging from cell sorting or directed delivery of therapeutic payloads.

Common catalytic (peroxide-driven) Au−Pt nanowire motors operate only in very low-ionic-strength aqueous media (owing to their self-electrophoretic mechanism) and hence cannot be applied to realistic biological and environmental matrices.[18] Catalytic microtube engines can display efficient motion in biological media, but require high concentrations of the hydrogen peroxide fuel.[8,23,24] The US nanomotors can be readily used in diverse high-ionic strength media (Figure 3). For example, efficient propulsion is observed in Figure 3b (and corresponding video SI 4) using untreated salt-rich seawater; the speed in this medium increases from 20 to 60 μm s^{-1} upon the raising of the applied voltages from 6 to 10 V (as compared to a 25 to 85 μm s^{-1} change in deionized

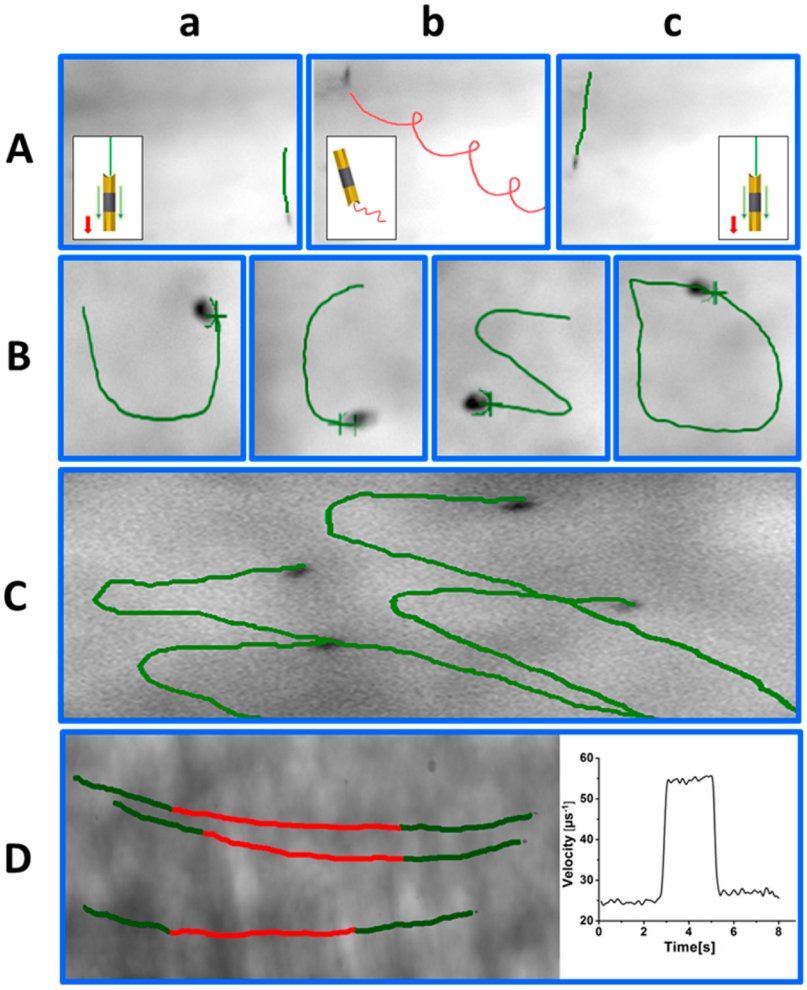

Figure 2. Magnetic guidance and movement behavior of ultrasound-propelled nanomotors. (A) Alignment of a nanomotor with a magnetic field (a), random motion of a nanomotor without a magnetic field (b), realignment with magnetic field (c). (B) Magnetically steered nanomotors along predetermined UCSD letters (route). (C) Coordinated motion of multiple US-powered magnetically guided nanomotors. (D) Speed modulation of multiple magnetically guided US-powered nanomotors in response to a 2.5 s 6−8−6 V potential step. Green and red track lines show the trajectories at applied potentials of 6 and 8 V, respectively. Inset (Right) shows the average motor speed *vs* time during such potential step. Conditions: media, deionized water; ultrasound field, 6 V and 2.51 MHz.

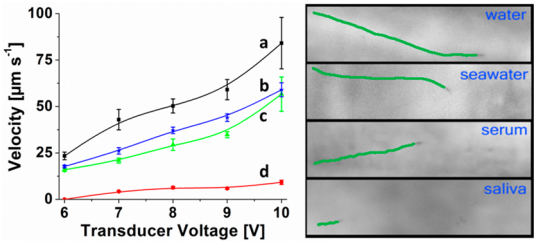

Figure 3. Dependence of nanomotor speed upon the ultrasound transducer voltage (power) in different media: (a) deionized water, (b) seawater, (c) serum, and (d) saliva. All samples were 20% (v/v) diluted. Measurements were carried out at 2.51 MHz using 1.8 μm-long Au/Ni/Au nanowires.

water; Figure 3a). The US-driven nanomotors also display efficient propulsion in complex biological environments, such as untreated serum (Figure 3c) and saliva (Figure 3d). Note, the substantial speed diminution observed in the saliva sample due to its high viscosity and complex molecular composition. Overall, the data of Figure 3 and SI Video 4 clearly indicate that US-driven nanomotors can operate in diverse environments and display a minimal salt effect. The nearly linear dependence of the speed upon the transducer voltage (indicated from Figure 3) offers a convenient control of the motor speed, including an on demand motor acceleration or deceleration. For example, Figure 2D and SI Video 5 illustrate the rapid (dynamic) change of the speed by modulating the transducer potential using a 6−8−6 V step of 2.5 s. Notice the instantaneous speed change from 25.1 to 54.6 and fast back to the original speed (~25 μm s^{-1}) upon stepping the potential up and down, respectively, demonstrating the controlled acceleration and deceleration capabilities of the acoustically driven nanovehicle.

We have also demonstrated a controllable concavity formation on the nanomotor using a sphere lithography technique to improve the asymmetric distribution

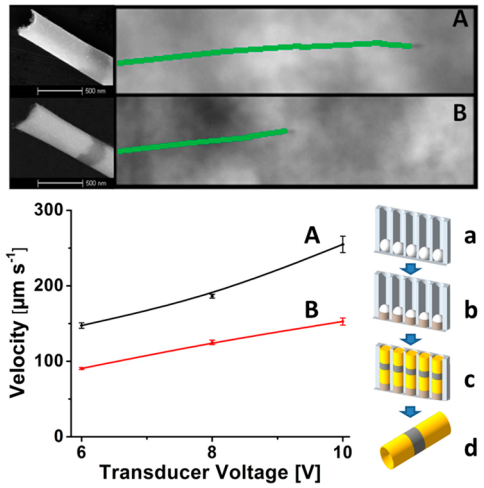

Figure 4. Propulsion behavior of nanomotors fabricated by different methods: dual-templating sphere lithography electrodeposition (A) and conventional template electrodeposition (B). Top: SEM images and "racing" tracklines of methods A and B under the same ultrasound field (6 V, 2.66 MHz). Bottom: (left) dependence of the motor speed upon the increasing ultrasound transducer voltage (2.66 MHz); (right) fabrication scheme coupling the membrane-template and sphere-lithography electrodeposition. (a) Infiltration of PS spheres into the membrane pores, (b) growth of sacrificial layer, (c) electrodeposition of Au/Ni/Au segments, and (d) release of the nanomotors from the dual template.

of the acoustic pressure and the propulsion performance. A previous report suggested that the concave shape is responsible for the axial propulsion of ultrasound-driven nanowire motors since scattering of acoustic waves from such cavities concentrates the energy near the curvature.[17] As illustrated in Figure 4 (bottom, right), the addition of a nanosphere template into the cylindrical nanopores of the membrane template, followed by electrodeposition of Au, Ni, and Au and subsequent dissolution of the PS nanospheres template, resulted in the formation of a nanoconcave shape at the bottom of the nanowires. The resulting distinct concave end facilitates the formation of the inside pressure gradient by the penetrating ultrasound waves, and the generation of the directional motion. The SEM images of Figure 4 (top, left) show the well-defined concave shape in the multisegment nanowire, fabricated by this technique, compared to common cavities created by the conventional membrane-template method.[17] This image illustrates that the inclusion of the sphere template during the electrodeposition creates a hemispherical-shaped cavity at the nanowire end. Such concavity formation results in an improved propulsion behavior, as indicated from Figure 4 which compares the speed of US-powered nanowire motors with (A) and without (B) using the sphere-lithography method at different transducer voltages (frequency of 2.66 MHz). For example, the use of the sphere lithographic method increases the nanomotor speed up to 67%, from 152.7 to 254.9 μm s^{-1}, (at a transducer voltage of 10 V). Such improvements are illustrated in Figure 4 (top, right) and SI Video 6 from the track-lines of a "race" of two nanomotors, fabricated by the two methods, under the same conditions. Clearly, a substantially faster speed is achieved using the motor fabricated by adding the sphere-lithographic step. We are currently investigating the optimal cavity geometry toward maximizing the propulsion efficiency.

So far we have demonstrated the enhanced directional magnetic movement of acoustically propelled Au–Ni–Au nanomotors and their ability to navigate in different biological media. The magnetic properties of the Ni segment can also facilitate the pick-up and transport of microsphere cargo along predetermined paths. The optical images of Figure 5A (and SI Video 7) illustrate such dynamic loading (b) and transport (c) of magnetic microspheres. The US-powered nanomotor can thus be magnetically guided to approach the target microsphere cargo at a speed of 17.8 μm s^{-1}. A dynamic loading of the microsphere onto the nanomotor is observed when the motor and the cargo sphere approach each other and display significant magnetic attraction. Subsequently, the nanomotor transports the microsphere with ~57% of its original speed (10.15 μm s^{-1}) along a predetermined path. The drag force F_D of this nanomotor can be calculated using Stokes eq 1 for a cylinder, with L (1.8 μm) and r (0.125 μm) being the length and radius of the nanomotors, respectively, μ being the viscosity of the fluid, and v being the nanomotor speed, thus resulting in a towing force of 0.093 pN.

$$F_D = \frac{2\pi\mu L v}{\ln\frac{L}{r} - 0.5} \quad (1)$$

Following the demonstration of the magnetic cargo pickup, we examined the functionalization of the US motors with different bioreceptors (such as antibody or lectin) toward the use of biomolecular interactions for selective capture processes. Previous studies of our group reported on the use of receptor-functionalized catalytic microtubular engines for isolating biological targets in a fuel-enhanced sample environment.[25–27] However, the peroxide-fuel requirement of such functionalized catalytic microengines may compromise the viability of the captured targets and the scope of such motor-based separations. In this study, we accomplished the motor-based target isolation (*e.g.*, bacteria capture and transport with both lectin and antibody-modified Au–Ni–Au nanomotors) without reliance on an external chemical fuel supply, hence ensuring the viability of the captured biological target.

Our new data indicate that, unlike the functionalization of catalytic micromotors,[26] the propulsion of US nanowire motors is hardly affected by their surface modification. For example, the nanowire

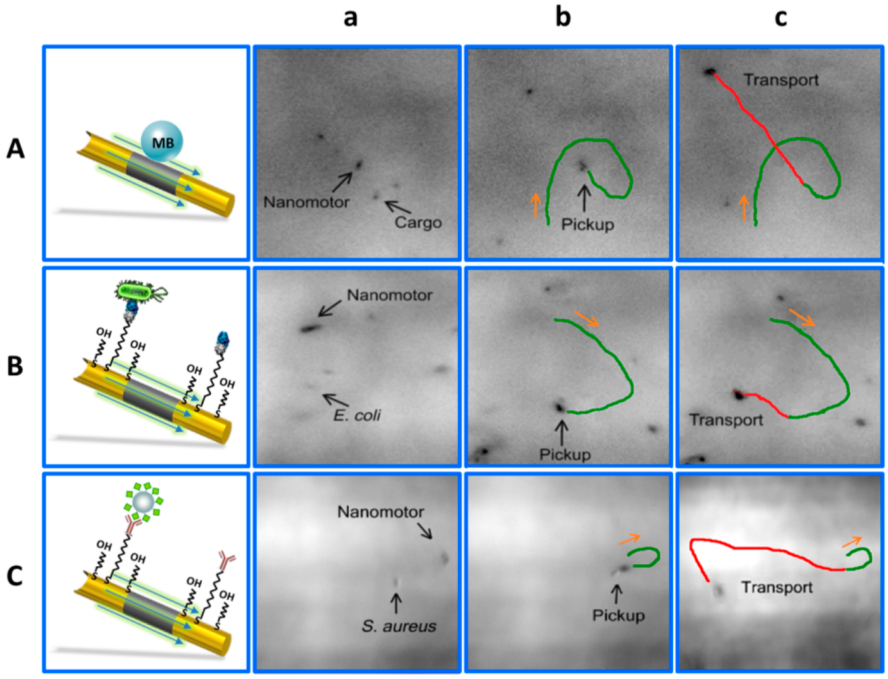

Figure 5. (A) Capture and transport of a 0.89 μm magnetic bead by an ultrasound-propelled Au/Ni/Au unmodified nanomotor approaching (a), capturing (b), and transporting (c) the magnetic particle. (B) Capture and transport of *E. coli* bacteria by a lectin-modified ultrasound-propelled nanomotor: (a) approaching, (b) pickup, and (c) transport the *E. coli* bacteria. (C) Capture and transport of *S. Aureus* bacteria by a Con A-modified ultrasound-propelled nanomotor: (a) approaching, (b) pickup, and (c) transport the *S. Aureus* bacteria. Conditions: media, deionized water (A) and PBS (pH 7.0) solutions (B and C); ultrasound field, 6 V and 2.51 MHz.

functionalization protocol was optimized for efficient lectin-bacteria interaction and transport. As illustrated in Figures 1 and 5, the receptor functionalization was accomplished by conjugating the lectin to the gold segments of the nanowire *via* a binary SAM. A MUA/MCH mixture created the binary SAM while 1-ethyl-3-(3-dimethylaminopropyl) carbodiimide (EDC)/*N*-hydroxysuccinimide (NHS) chemistry served for activating the MUA carboxyl groups for conjugation with ConA (see Experimental Section for additional details). To promote favorable target accessibility while minimizing nonspecific adsorption, the binary SAM was prepared using 0.25 mM MUA and 0.75 mM MCH as optimal alkanethiol concentrations.[26] Such modification of the nanowire surface has a negligible effect upon their speed (25 μm s^{-1} V *vs* 26 μm s^{-1} at 6 V and 2.51 MHz). Following the SAM activation, the lectin receptor was immobilized *via* EDC/NHS coupling using a binding buffer (BB) solution containing 9 mg/mL of ConA. The speed of the resulting lectin-modified nanowire motor (25 μm s^{-1}) is similar to that of the uncoated gold-wire motor, which corresponds to a force of 0.13 pN (on the basis of eq 1). In contrast, a substantial reduction in locomotion speed and hence the towing capabilities of chemically propelled nanomotors have been reported after their SAM modification and bioreceptor functionalization processes.[26] Overall, the high speed of the modified US-based micromotors, their high cargo towing capacity, and the strong lectin/bacteria interaction ensure efficient pick-up and transport of the target bacteria.

Figure 5B and SI Video 8 illustrate an "on-the-fly" capture of the *E. coli* bacteria target by the ConA-functionalized US-driven nanowires, based on binding of the ConA receptor to the O-antigen of the *E. coli* cell wall. The lectin-functionalized nanomotor is magnetically guided in the bacteria-containing PBS media and approaches the *E. coli* cell at a speed of 21.85 μm s^{-1} (b); the bacterium is instantaneously captured and transported (c) over a preselected trajectory at a decreased nanomotor speed of 12.35 μm s^{-1} (*i.e.*, around 56% of the original speed), corresponding to a towing force of 0.114 pN. Notice that the similar size of the *E. coli* bacterium (0.6 $\times$ 2 μm) and nanowire motor allows convenient direct visualization of the binding event. If it is assumed that the bacterium is a sphere with a radius (r) of 0.7 μm, a drag force (F_{Dcell}) of 0.037 pN can be estimated for transporting it at a speed (v) of two body lengths s^{-1} based on the Stokes equation ($F_{Dcell} = 6\pi\mu rv$). Such transport of large biological targets demonstrates the strong towing force of the ultrasound-propelled nanowires. In addition, it is possible to further increase the towing force on demand up to 0.4 pN by increasing the power of the ultrasound waves. No capture of the bacteria target was observed in controlled experiments involving unmodified nanomotors interacting with *E. coli,* even after numerous (>30) motor-cell contacts. These data

indicate the absence of nonspecific binding and demonstrate the specificity of the functionalized US-driven micromotors.

To extend the application of ultrasound-powered micromotors toward the isolation of biological targets, the Au–Ni nanowires were functionalized with antiprotein A antibody toward the capture and transport of *Staphylococcus aureus (S. aureus)* bacteria. The antibody functionalization was achieved by using a similar EDC/NHS coupling chemistry, through binary SAM of alkanethiols (used for attaching the ConA lectin receptor; see Experimental Section for specific details, based on the optimal antibody functionalization used for chemically powered motors[27]). Unlike catalytic-propelled antibody-modified engines, whose functionalization with protein A antibodies resulted in major speed diminutions,[27] the speed of the Ab-SAM modified ultrasound micromotors was not affected by the surface functionalization. Figure 5C and SI Video 9 illustrate the pick-up of a *S. aureus* bacterium by the US-powered antibody-modified nanowire. Such capture and transport is based on the affinity of the surface-bound antiprotein A antibody to protein A present in the bacterial cellular wall. As expected, the initial speed of the nanomotor, 29.6 μm s^{-1} (corresponding to a drag force of 0.166 pN) decreases to 16.3 μm s^{-1}, after capturing the 2 μm *S. aureus* bacterium. Overall, the data of Figure 5 panels B and C demonstrate the ability of US-micromotors, functionalized with different bioreceptors, to capture and isolate various biological targets. The ultrasound-driven (fuel-free) operation is advantageous over common peroxide-powered functionalized micromotors toward maintaining the viability of the captured biological targets.

Drug delivery capability is also demonstrated by these biocompatible nanodevices. A electropolymerized polypyrrole-polystyrene sulfonate (PPy-PSS) segment, added to the previously described Au–Ni–Au nanowire motor, serves as a carrier for the brilliant green (BG) model antiseptic drug (Figure 6). This positively charged drug is retained *via* electrostatic forces to the surface of the negatively charged PPy-PSS polymeric backbone.[28,29] A pH-sensitive triggered BG release is achieved when change to an acidic media (of pH 4) occurs and hence the PPy-PSS "carrier" is protonated. The SEM image of Figure 6A clearly illustrates the new PPy-PSS/BG segment, along with the Au, Ni, and Au segments, and indicates that the polymer segment is well-connected to the Au segment. The temporal profile of Figure 6B illustrates the pH-triggered release of BG, demonstrating the rapid release of 78% of the BG drug within 30 min at pH 4, and up to 95% release within 120 min. A control experiment using the original physiological pH of 7.4 over the same 30 min period displays a greatly diminished (25%) drug release, and a nearly similar limited release

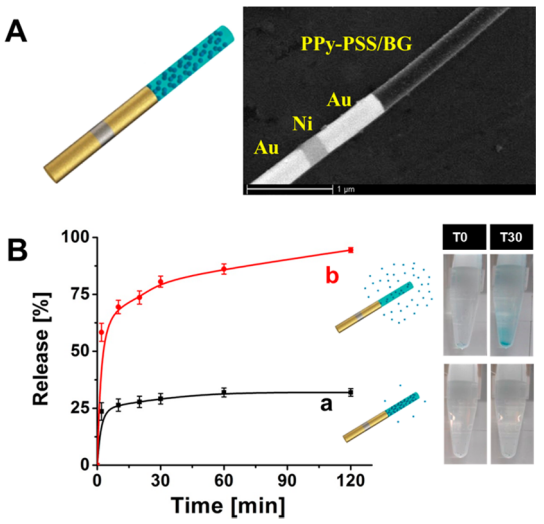

Figure 6. Characterization of ultrasound-propelled nanowire motor containing the pH-responsive drug-loaded polymeric segment: (A) SEM image of the Au/Ni/Au/PPy-PSS nanowire. (B) Time-dependent release of BG at pH 7.4 (a) and 4.0 (b). Right: optical images of the release of BG particles at 0 and 30 min (left and right) using pH 4.0 (top) and 7.4 (bottom).

over the entire 120 min period. Unlike catalytic nanowire motors transporting drug-loaded PLGA particles that displayed a diminished speed in the presence of the drug carrier,[30] only a negligible change of the speed of the ultrasound-powered motor was observed upon addition of the drug-conjugated PPy-PSS segment to the initial Au/Ni/Au motor design. The latter reflects the streamlined shape of the built-in drug carrier segment. These multisegment motors also retained their structural integrity, with no apparent separation of their segments after a 30 min exposure to the operational ultrasound radiation.

CONCLUSIONS

We have demonstrated acoustically driven nanowire motors with enhanced capabilities, design, performance, and functionalities, including magnetic guidance, coordinated motion, cargo towing, sorting of biological targets, drug delivery, operation in diverse media, and improved speed *via* the dual-templating fabrication technique. These new capabilities have been realized by incorporating magnetic Ni and drug-loaded segments, and by conjugating different bioreceptors to the gold segments. Such Au/Ni/Au/PPy nanowire motors have been prepared using a simple template electrodeposition protocol. The added Ni segment offers guided movement along preselected paths as well as collective motion of multiple US-driven motors. In addition, sphere lithography has been used to improve the concavity formation at one end of the wire and thus to enhance speed and power. Further studies are desired for identifying the ideal cavity geometry for maximizing the acoustic pressure and optimizing the propulsion force. The functionalization

with various bioreceptors has allowed, for the first time, the use of acoustically driven nanomotors for capturing and isolating biological targets. Efficient movement has been obtained in complex biological and environmental media. pH-induced drug release from the polymeric segment has also been demonstrated. The coupling of receptor functionalization and a drug-releasing segment makes these versatile US-driven motors the first example of a theranostics (therapeutic/diagnostic) nanomotor device. Such coupling of multiple functionalities into a single nanoscale machine thus streamlines potential biomedical applications. With further improvements and additional functionalities, ultrasound-driven nanomotors are expected to perform diverse and complex operations in a variety of important fields.

EXPERIMENTAL SECTION

Reagents and Solutions. 6-Mercaptohexanol (MCH), 11-mercaptoundecanoic acid (MUA), *N*-hydroxysuccinimide (NHS), 1-(3-dimethylaminopropyl)-*N*′-ethylcarbodiimide hydrochloride (EDC), lectin from *Canavalia ensiformes* (Concanavalin A, ConA), acetic acid sodium salt, ethanolamine, 2-(*N*-morpholino) ethanesulfonic acid (MES), $CaCl_2$, and $MnCl_2$ were purchased from Sigma-Aldrich. The BB solution consisted of a 0.1 M acetate buffer (pH 5.0), containing 1 mM Mn^{2+} and 1 mM Ca^{2+}. These two divalent metals are necessary in order to get an active ConA conformation for its binding to carbohydrates as reported.[26] A 0.1 M MES buffer solution (pH 5.0) was used in the carboxylic activation step. A 1 M ethanolamine solution (pH 8.5) served as a blocking agent for the amine reactive-esters. All chemicals were analytical-grade reagents and were used as received without any further purification and prepared by dilution in 18.2 MΩ cm Milli-Q deionized water when not otherwise specified. Experiments were carried out at room temperature.

Bacterial strains of *E. coli* NEB 5-α (New England Biolabs, Ipswich, MA) were obtained from the Clinical Microbiology Laboratory, University of California Los Angeles (UCLA), with approval from the UCLA and Veterans Affairs institutional review boards and appropriate Health Insurance Portability and Accountability Act exemptions. The pellets were received in centrifuge tubes and were stored at −80 °C until use. Overnight bacterial cultures were freshly inoculated into Luria broth (LB) and grown to logarithmic phase as measured by the optical density at 600 nm. Concentrations of the specimen (over the logarithmic phase) were determined by serial plating. *S. aureus* cells (10% wet w/v of essentially nonviable *S. aureus* Cowan strain cells in 0.04 M sodium phosphate buffer (pH 7.2, 0.15 M NaCl) containing 0.05% NaN_3) were supplied by Sigma, and *S. cerevisiae* were obtained from Science Stuff. Human serum was purchased from Sigma; saliva samples were collected daily, drinking water was purchased in a local supermarket while seawater samples (pH ≈ 8) were collected from the shores of La Jolla, CA. All these real samples were spiked with the appropriate concentration of bacteria at the moment of the experiment.

Synthesis of the Metallic Nanowires. The nanowire motors were prepared by a common template-directed electrodeposition protocol. A silver film was first sputtered on one side of the porous alumina membrane template containing 200-nm-diameter cylindrical pores (catalogue no. 6809-6022; Whatman, Maidstone, UK) to serve as a working electrode. The membrane was then assembled in a plating cell with an aluminum foil serving as a contact for the sputtered silver. Copper was initially electrodeposited in the membrane from a $CuSO_4 \cdot 5H_2O$ (1 M) solution, using a charge of 8 C and a potential of −0.95 V (*vs* a Ag/AgCl reference electrode, along with a Pt-wire counter electrode). The removal of this sacrificial layer helps to create the concave shape in one end of the wire motor. Subsequently, gold was plated from a commercial gold plating solution (Orotemp 24 RTU RACK; Technic Inc.) at −0.95 V (*vs* Ag/AgCl), using a charge of 1 C; nickel was deposited from a nickel plating solution containing $NiCl_2 \cdot 6H_2O$ (20 g L^{-1}), $Ni(H_2NSO_3)_2 \cdot 4H_2O$ (515 g L^{-1}), and H_3BO_3 (20 g L^{-1}) at −0.95 V (*vs* Ag/AgCl) for 1 C; and finally gold was deposited using a charge of 1 C. The sputtered silver layer and copper sacrificial layer were mechanically removed from the membrane by polishing with 3−4 μm alumina slurry, followed by dissolution of any remaining silver and copper with 8 M HNO_3. The membrane was then dissolved in a 3 M NaOH solution for 30 min to completely release the nanowires. The nanowires were collected by centrifugation at 6000 rpm for 5 min and were washed repeatedly with nanopure water (18.2 MΩ cm) until a neutral pH was achieved. All nanowires were stored in 1 mL of nanopure water at room temperature.

A dual-templating approach was used for fabrication of a controllable concave size at the end of the nanowires. A 3 μL sample of PS spheres (2.5% w/v) with a diameter of 200 nm (Spherotech, Inc., IL) was diluted with 20 mL of water and filled into the silver-sputtered membrane pores. These nanospheres were used as a second sacrificial template to enhance the concavity. After infiltration of PS spheres into the pores, the membrane was placed in a plating cell and was used for nanowires fabrication as mentioned above.

Drug-loaded nanomotors were prepared by using the same template-assisted electrodeposition protocol of Au/Ni/Au nanowires (described earlier) followed by the addition of a polypyrrole-polystyrene sulfonate (PPy-PSS) composite segment by subsequent electropolymerization from a solution containing 0.15 M of distilled pyrrole 98% and 50 mM of poly(sodium 4-styrene sulfonate) in PBS buffer solution pH 7.2 using a charge of 0.5 C at a potential of 0.8 V. The Brilliant Green (BG) drug was loaded onto PPy-PSS nanomotor segment by a 2 h incubation of 50 μL of the nanowire solution into 1 mL of 0.2 mM BG solution. The drug-loaded PPy/Au/Ni/Au nanomotors were then collected by a 5 min centrifugation at 8000 rpm and were washed repeatedly with nanopure water (18.2 MΩ cm) to remove all unconjugated drug molecules from the nanomotor solution. The drug-conjugated nanomotors were then added to PBS buffer solutions at pH 4.0 and pH 7.4 to test the pH-induced drug release. UV spectra, recorded after different time intervals were used for estimating the amount of drug released. The presence of BG in the solution was indicated from the absorbance peak at 620 nm.

Ultrasound Setup. The ultrasonic experiments were carried out in a cell similar to that described by Mallouk.[17] The cell was made in a stainless steel plate 5 mm × 5 mm × 0.94 mm, covered by four layers of 60 μm Kapton tape with a center hole of 6 mm in diameter and 240 μm height as the sample reservoir, covered by a 18 × 18 × 0.15 mm cover slide for reflection of the ultrasound waves and for stability of the solution (avoid motion of the solution due to disturbances of the environment). The piezoelectric transducer which produces the ultrasound waves (Ferroperm PZ26 disk 10 mm diameter × 0.5 mm thickness) was attached to the bottom center of the stainless steel plate. The continuous ultrasound sine wave was applied *via* a piezoelectric transducer, through an Agilent 15 MHz arbitrary waveform generator, in connection to a homemade power amplifier. The applied waveform was a continuous sine wave with a frequency of 2.51 (or 2.66) MHz and voltage amplitude varying between 6 and 10 V as needed for controlling the intensity of the ultrasonic wave. The electric signal was monitored by a 20 MHz Tektronix 434 storage oscilloscope. The motion of the nanomotors was visualized with a Nikon Eclipse 80i, 20X objective illuminated with a Nikon MKII fiber optics light. The images were acquired at 10 frames/s with a PhotometricsCoolSnap HQ^2 1392 × 1040 pixels CCD camera attached to the

microscope and were processed with Metamorph 7.7.5 software (Molecular Devices, Sunnyvale, CA).

Nanowires Functionalization. Nanowires were functionalized with either lectin protein receptors for the capture and transport of *E. coli* or with antiprotein A antibody for *S. aureus* loading, respectively. The external gold surface of the nanowires was modified by an overnight immersion in a binary mixture of 0.25 mM of MUA and 0.75 mM of MCH thiols in absolute ethanol (200 Proof). After washing with Milli-Q water, the surface-bound MUA carboxylic moieties were activated with a 20 mM NHS and 10 mM EDC in 0.1 M MES buffer solution pH 6.5 for 30 min and washed with BB or PBS solution, respectively, for 1 min. Functionalization of the motors with the lectin protein receptors was achieved by immersing the wires in a BB solution containing 9 mg/mL of ConA receptor for 2 h. Antibodies receptors were immersed in 100 μL of anti-Prot-A antibody, diluted in PBS (1×) pH 7.2, to a final concentration 750 μg/mL for 2 h. In both cases, the remaining amine reactive-esters of the activated monolayer were blocked with 1 M ethanolamine solution, pH 8.5, for 30 min and later resuspended in BB solution or PBS for lectins or antibodies, respectively. Between each incubation and washing steps the nanomotors were isolated by centrifugation at 6000 rpm for 4 min; all experiments were carried out at room temperature. Control nanowires (without any receptor) were prepared using the same protocol (with the SAM assembly, activation, and blocking steps) but without adding the Con A and antibody, while carrying out the corresponding incubation in BB or PBS, respectively.

Identification and Isolation of Target Bacteria. For the detection and isolation of the target bacteria, a mixture of 1.5 μL of solution of the modified-nanomotors and 1 μL of the diluted bacterial cell suspension (prepared in the sample matrix, in the BB or PBS solution) was dropped onto a cleaned ultrasound reservoir and covered by a coverslide (see the setup description). The feasibility to capture *E. coli* and *S. aureus* bacteria was tested directly by magnetic guidance of the lectin (or antiprotein A) modified wires toward the target cells, respectively. The recognition event was monitored by videos captured with a Nikon Eclipse 80i upright microscope and a CoolSNAP HQ^2 camera, 20× objective (unless mentioned otherwise) and acquired at a frame rate of 10 frames/s using the Metamorph 7.7 software (Molecular Devices, Sunnyvale, CA). Capture and transport of bacteria were carried out by adding the lectin-based and antibody-based nanomotors in undiluted samples containing appropriate concentration of the bacteria and the corresponding buffer.

Conflict of Interest: The authors declare no competing financial interest.

Supporting Information Available: Figure S1. Videos: magnetic *vs* nonmagnetic guidance switch; ultrasonic propulsion with magnetic guidance; coordinated motion of nanomotors; speed of nanomotors in different media; nanomotor speed modulation; speed of nanomotors with different fabrication techniques; magnetic bead capture; *E. coli* capture; *S. aureus* capture. This material is available free of charge via the Internet at http://pubs.acs.org.

Acknowledgment. This project received support from the Defense Threat Reduction Agency-Joint Science and Technology Office for Chemical and Biological Defense (Grant No. HDTRA1-13-1-0002). V.G. is on leave and acknowledges financial support from Centro de Nanociencias y Nanotecnología UNAM and DGAPA-UNAM fellowship (Mexico). W.G. is a HHMI International Student Research fellow. The authors thank D. Wiitala for his assistance.

REFERENCES AND NOTES

1. Paxton, W. F.; Sundararajan, S.; Mallouk, T. E.; Sen, A. Chemical Locomotion. *Angew. Chem., Int. Ed.* **2006**, *45*, 5420–5429.
2. Ozin, G. A.; Manners, I.; Fournier-Bidoz, S.; Arsenault, A. Dream Nanomachines. *Adv. Mater.* **2005**, *17*, 3011–3018.
3. Mallouk, T. E.; Sen, A. Powering Nanorobots. *Sci. Am.* **2009**, *300*, 72–77.
4. Wang, J. Can Man-Made Nanomachines Compete with Nature Biomotors?. *ACS Nano* **2009**, *3*, 4–9.
5. Nelson, B. J.; Kaliakatsos, I. K.; Abbott, J. J. Microrobots for Minimally Invasive Medicine. *Annu. Rev. Biomed. Eng.* **2010**, *12*, 55–85.
6. Wang, J. *Nanomachines: Fundamentals and Applications*, Wiley-VCH: Weinheim, Germany, 2013, ISBN 978-3-527-33120-8.
7. Mirkovic, T.; Zacharia, N. S.; Scholes, G. D.; Ozin, G. A. Fuel for Thought: Chemically Powered Nanomotors Out-Swim Nature's Flagellated Bacteria. *ACS Nano* **2010**, *4*, 1782–1789.
8. Mei, Y.; Solovev, A. A.; Sanchez, S.; Schmidt, O. G. Rolled-up Nanotech on Polymers: From Basic Perception to Self-Propelled Catalytic Microengines. *Chem. Soc. Rev.* **2011**, *40*, 2109–2119.
9. Pumera, M. Electrochemically Powered Self-Propelled Electrophoretic Nanosubmarines. *Nanoscale* **2010**, *2*, 1643–1649.
10. Zhang, L.; Abbott, J. J.; Dong, L.; Peyer, K. E.; Kratochvil, B. E.; Zhang, H.; Bergeles, C.; Nelson, B. J. Characterizing the Swimming Properties of Artificial Bacterial Flagella. *Nano Lett.* **2009**, *9*, 3663–3667.
11. Ghosh, A.; Fischer, P. Controlled Propulsion of Artificial Magnetic Nanostructured Propellers. *Nano Lett.* **2009**, *9*, 2243–2245.
12. Gao, W.; Sattayasamitsathit, S.; Manesh, K. M.; Weihs, D.; Wang, J. Magnetically Powered Flexible Metal Nanowire Motors. *J. Am. Chem. Soc.* **2010**, *132*, 14403–14405.
13. Chang, S. T.; Paunov, V. N.; Petsev, D. N.; Velev, O. D. Remotely Powered Self-Propelling Particles and Micropumps based on Miniature Diodes. *Nat. Mater.* **2007**, *6*, 235–240.
14. Calvo-Marzal, P.; Sattayasamitsathit, S.; Balasubramanian, S.; Windmiller, J. R.; Dao, C.; Wang, J. Propulsion of Nanowire Diodes. *Chem. Commun.* **2010**, *46*, 1623–1624.
15. Loget, G.; Kuhn, A. Electric Field-induced Chemical Locomotion of Conducting Objects. *Nat. Commun.* **2011**, *2*, 535.
16. Kagan, D.; Benchimol, M. J.; Claussen, J. C.; Chuluun-Erdene, E.; Esener, S.; Wang, J. Acoustic Droplet Vaporization and Propulsion of Perfluorocarbon-Loaded Microbulletsfor Targeted Tissue Penetration and Deformation. *Angew. Chem., Int. Ed.* **2012**, *51*, 7510–7522.
17. Wang, W.; Castro, L. A.; Hoyos, M.; Mallouk, T. E. Autonomous Motion of Metallic Microrods Propelled by Ultrasound. *ACS Nano* **2012**, *6*, 6122–6132.
18. Wang, J.; Gao, W. Nano/Microscale Motors: Biomedical Opportunities and Challenges. *ACS Nano* **2012**, *6*, 5745–5751.
19. Ziskin, M. C.; Petitti, D. B. Epidemiology of Human Exposure to Ultrasound: A Critical Review. *Ultrasound Med. Biol.* **1988**, *14*, 91–96.
20. Reece, E. A.; Assimakopoulos, E.; Zheng, X. Z.; Hagay, Z.; Hobbins, J. C. The Safety of Obstetric Ultrasonography: Concern for the Fetus. *Obstet. Gynecol.* **1990**, *76*, 139–146.
21. Kline, T. R.; Paxton, W. F.; Mallouk, T. E.; Sen, A. Catalytic Nanomotors: Remote-Controlled Autonomous Movement of Striped Metallic Nanorods. *Angew. Chem., Int. Ed.* **2005**, *44*, 744–746.
22. Burdick, J.; Laocharoensuk, R.; Wheat, P. M.; Posner, J. D.; Wang, J. Synthetic Nanomotors in Microchannel Networks: Directional MicrochipMotion and Controlled Manipulation of Cargo. *J. Am. Chem. Soc.* **2008**, *130*, 8164–8165.
23. Gao, W.; Sattayasamitsathit, S.; Orozco, J.; Wang, J. Highly Efficient Catalytic Microengines: Template Electrosynthesis of Polyaniline/Platinum Microtubes. *J. Am. Chem. Soc.* **2011**, *133*, 11862–11864.
24. Manesh, K. M.; Cardona, M.; Yuan, R.; Clark, M.; Kagan, D.; Balasubramanian, S.; Wang, J. Template-Assisted Fabrication of Salt-Independent Catalytic Tubular Microengines. *ACS Nano* **2010**, *4*, 1799–1804.
25. Campuzano, S.; Kagan, D.; Orozco, J.; Wang, J. Motion-Driven Sensing and Biosensing Using Electrochemically Propelled Nanomotors. *Analyst* **2011**, *136*, 4621–4630.

26. Campuzano, S.; Orozco, J.; Kagan, D.; Guix, M.; Gao, W.; Sattayasamitsathit, S.; Claussen, J. C.; Merkoci, A.; Wang, J. Bacterial Isolation by Lectin-Modified Microengines. *Nano Lett.* **2012**, *12*, 396–401.
27. Garcia, M.; Orozco, J.; Guix, M.; Gao, W.; Sattayasamitsathit, S.; Escarpa, A.; Merkoci, A.; Wang, J. Micromotor-Based Lab-on-Chip Immunoassays. *Nanoscale* **2013**, *5*, 1325–1331.
28. Bhasikuttan, A. C.; Mohanty, J.; Nau, W. M.; Pal, H. Efficient Fluorescence Enhancement and Cooperative Binding of an Organic Dye in a Supra-Biomolecular Host−Protein Assembly. *Angew. Chem., Int. Ed.* **2007**, *46*, 4120–4122.
29. Baker, C. K.; Qiu, Y.-J.; Reynolds, J. R. Electrochemically Induced Charge and Mass Transport in Polypyrrole/Poly-(styrenesutfonate) Molecular Composites. *J. Phys. Chem.* **1991**, *95*, 4446–4452.
30. Kagan, D.; Laocharoensuk, R.; Zimmerman, M.; Clawson, C.; Balasubramanian, S.; Kang, D.; Bishop, D.; Sattayasamitsathit, S.; Zhang, L.; Wang, J. Rapid Delivery of Drug Carriers Propelled and Navigated by Catalytic Nanoshuttles. *Small* **2010**, *6*, 2741–2747.